Contents lists available at ScienceDirect

International Journal of Adhesion and Adhesives

journal homepage: www.elsevier.com/locate/ijadhadh

Micromechanical influence of near-surface adherend morphology and bondline fillers on the strain distribution in shear-loaded composite bonds

Jörg Gregor Diez [a,b,*], Jens Holtmannspötter [b], Elisa Arikan [b], Philipp Höfer [a]

[a] University of the Bundeswehr Munich – Department of Aerospace Engineering, Institute of Lightweight Engineering, Werner-Heisenberg-Weg 39, 85577, Neubiberg, Germany
[b] Bundeswehr Research Institute for Materials, Fuels and Lubricants (WIWeB), Institutsweg 1, 85435, Erding, Germany

ARTICLE INFO

ABSTRACT

The near-surface morphology in the joining areas of adherends has a significant impact on the fatigue behavior of adhesively bonded composites. In the production process of composites, numerous opportunities exist for dictating surface morphology through the utilization of different top-layer semi-finished products. For instance, release films and peel ply fabrics can be employed to modulate the thickness and topography of the upper resin layer. These materials are subsequently removed prior to the further processing and assembly of the composites, leaving their negative imprint on the material surface. The resultant structures typically exhibit dimensions on the scale of a few micrometers. Another component in adhesive bonds are fillers, which have diameters in the same size range. Both adherend morphology and fillers influence the macroscopic behavior of the bonded joint. By *in situ* examining bonded end-notched flexure specimens inside a scanning electron microscope, the adhesive layer and the near-surface region of the adherends can be observed in detail under load. Evaluating these scanning electron microscope images using digital image correlation enables quantitative analysis of the strain distribution within the micrometer range. This allows the identification of the effects the adherend's near-surface morphology and the composition of the bondline (e.g. fillers, meshes) have on the shear strain distribution along bondlines. Consequently, conclusions can be drawn regarding their influence on the service life of adhesive bonds.

1. Introduction

Carbon fiber-reinforced plastics (CFRP) are distinguished by their high strength and stiffness combined with low weight. This makes them an ideal lightweight material for constructing structures with maximum performance and efficiency. For this reason, carbon fiber-reinforced plastics have become well established as a material for aircraft structures in recent years [1,2].

Composites are formed through the combination of two distinct materials: fibers embedded within a matrix material. Mostly, this involves carbon fibers embedded within a thermosetting polymer matrix. When employing infiltration processes as well as pre-impregnated material (prepreg), the surface morphology of the CFRP substrate can be precisely engineered using different semi-finished products, such as release films and peel plies [3].

To benefit from the lightweight construction potential of composites,

a material-specific joining process is required. Adhesive bonding offers distinct advantages over conventional methods such as riveting. It allows the joining of thin-walled structures, comes with less weakening of the adherends, uniform stress distribution and high dynamic strength of the bonds [4].

However, for the application of structural adhesive bonding in aviation, reliable bonded joints are required. Achieving this necessitates ensuring the reliable prediction of the long-term behavior of the joints. Previous studies indicate that the service life of bonded CFRP test specimens is influenced by their surface morphology [5]. This raises the question of how the joining areas (comprising the adhesive layer and near-surface region) in adhesive joints of fiber-reinforced plastics should be configured to ensure a long service life of the bonded joints.

To gain a deeper insight into the micromechanical processes within an adhesive bond and their impact on service life, studies at appropriate size scales are crucial as they offer a higher level of insight compared to
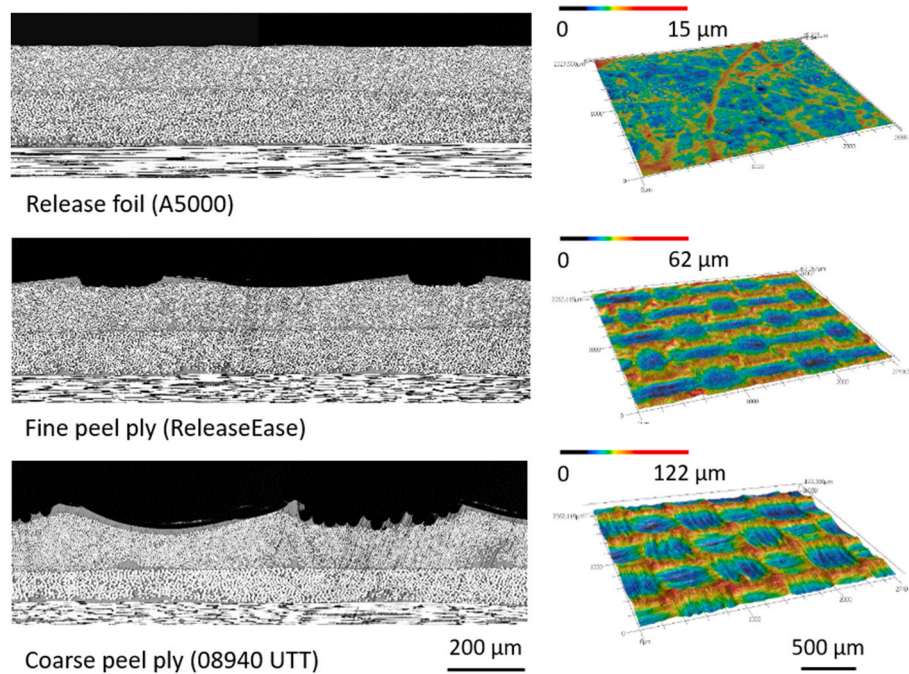
Fig. 1. Cross-sections and 3D top views of CFRP laminates produced using different semi-finished products (CLSM images).

traditional test specimens. Consequently, miniaturized test specimens were subjected to testing under a scanning electron microscope (SEM) and analyzed using digital image correlation (DIC).

This study investigates the influence of fillers and the surface morphology on strain distribution in the region adjacent to the adhesive layer. The utilization of small end-notched flexure specimens (ENF) enables the precise application of shear load in the bond. Because of the artificial crack present in this specimen type, the location of the highest load and consequently the site of damage initiation is predetermined, thereby facilitating microscopic examination at high resolutions.

2. Materials and methods

2.1. Manufacturing of CFRP

The high strength of carbon fibers stems from their graphite structure predominantly oriented parallel to the fiber axis. Single fibers have a diameter of 5–10 µm, and thousands of them are assembled into a roving for further application [3]. The matrix material can be either a thermoset or a thermoplastic polymer. Traditionally, thermosets are more common, which are typically made of epoxy resin for high-performance

applications such as in aviation [6].

When CFRP is utilized in the manufacturing process in the form of prepreg, the fiber rovings have already been impregnated with the matrix material (preimpregnated). In this case, however, the matrix is not yet polymerized. The unidirectional prepreg sheets are arranged into the desired shape on a suitable tool before the matrix undergoes cross-linking. Here, the layer structure of the laminate is determined by the required macroscopic properties of the component. In this study, a quasi-isotropic layer structure with $[0/+45/90/-45]_s$ orientation of the material Hexcel HexPly 8552/IM7 (Hexcel Corporation, Stamford/CT, USA) was employed.

The laminate was manufactured using the vacuum bag molding process. For this purpose, the prepreg is positioned on a mold coated with release agent, with a release film or peel ply placed on the top layer. A bleeder ply is placed on top to absorb excess resin from the laminate, followed by a breather ply made of nonwoven fabric. Finally, a vacuum bag is positioned over this assembly and connected to a vacuum pump which applies a pressure of −0.093 MPa to the assembly [6,7]. The curing of the laminate within the vacuumed structure is conducted in accordance with the manufacturer's specifications at 180 °C in an autoclave operating at 0.5 MPa [8].
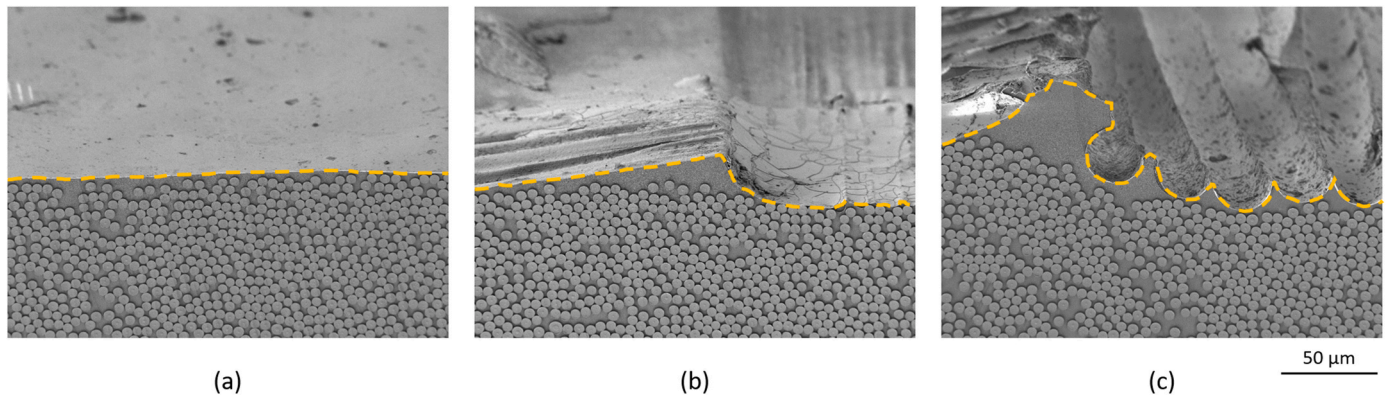

Fig. 2. Magnified representations of the characteristic features of each surface morphology (SEM images of cross-sections after ion-polishing). (a) Release foil A5000. (b) Peel ply ReleaseEase. (c) Peel ply 08940 UTT.
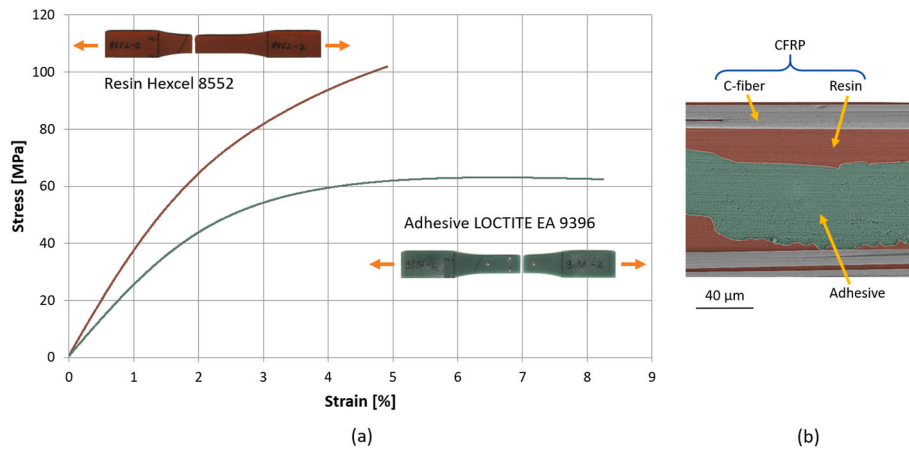
Fig. 3. (a) Representative stress-strain curves of the tensile tests on resin 8552 and adhesive LOCTITE EA 9396. (b) Close-up SEM cross-section image of a CFRP bond with color highlighting of its individual components.

There are at least three reasons for using a release film or peel ply: firstly, it ensures protection of the CFRP surface during transportation, storage, and processing, safeguarding it against substances such as release agents. Additionally, it sponges-up surplus resin and creates a defined surface structure that, in conjunction with an appropriate pre-treatment method, ensures good bondability [9–11]. Surface pre-treatment is essential here, as most peel plies are coated with a release agent so that they can be peeled off the surface. Otherwise, peeling would damage the surface too much and possibly tear out carbon fibers. However, this results in the CFRP surface being contaminated. A possibility to remove this contamination and ensure good bondability is, for example, a plasma process [12].

Additionally, the selection of this semi-finished product significantly influences the surface morphology of the CFRP, as it leaves its negative imprint on the surface when peeled off. Thereby, the amount of resin at the surface, the surface geometry and the distribution of the fibers in the near-surface region is affected. The following aerospace common release films and peel plies were used in this study: the smooth release film A5000 from Diatex SAS (Saint-Genis-Laval, France), made of fluorinated ethylene propylene, as well as two peel plies with different fabric fineness in a plain weave. The finer peel ply, ReleaseEase by Airtech Europe Sarl (Differdange, Luxembourg), is comprised of glass fibers coated with PTFE release agent. The coarser peel ply 08940 from UTT Indorama Ventures Mobility Krumbach GmbH & Co. KG (Krumbach, Germany) is made of Nylon.

Fig. 1 displays cross-sections of the CFRP laminates produced using different semi-finished products. The images were captured using a confocal laser scanning microscope (CLSM), revealing distinct differences in surface roughness.

In Fig. 2, the characteristic features of each surface morphology are magnified. It shows images that are captured by a SEM, with the specimens tilted at 20°. The upper edge of the test specimens in the cross-section was highlighted with a yellow line for clarity. The cross-sections of the specimens under investigation were prepared using an ion polisher, as suggested by Holtmannspötter et al. [13]. Sub-image (a) illustrates that the smooth release film produces a very flat surface with a continuous thin resin layer, with the carbon fibers lying almost flush with each other. When using the ReleaseEase peel ply (sub-image (b)), it leaves its negative imprint on the CFRP surface. This creates continuously rising flanks, indicating areas with resin accumulations devoid of carbon fibers. With the significantly coarser 08940 UTT peel ply (sub--image (c)), sharp protrusions and large areas with resin accumulations become visible. Additionally, partial displacement of carbon fibers from the surface can be observed in some specimens.

2.2. Manufacturing of the ENF test specimens

For investigating the influence of shear loading on an adhesive bond, ENF specimens present an advantageous alternative to the commonly employed single-lap shear specimens, especially due to the more uniform stress distribution. Furthermore, the area of damage initiation is predetermined by the unilateral notch beforehand.

During the fabrication of the ENF specimens, two CFRP laminates, each with a thickness of 1 mm, were bonded together using a fixture. To create the artificial crack, metal strips coated with a release agent were inserted into the adhesive bond. These strips also serve to adjust the adhesive layer thickness. Metal strips of both 20 μm and 80 μm were utilized. The detailed procedure for the fabrication and preparation of the ENF specimens is described in Diez et al. [14].

For this investigation, three different adhesives were used. Two of them are paste epoxy adhesives from Henkel (Henkel AG & Co. KGaA, Düsseldorf, Germany) (LOCTITE EA 9395 [15] and LOCTITE EA 9396 [16]), both based on Bisphenol A. The difference between the two systems is that the LOCTITE EA 9395 adhesive contains silicate fillers with a diameter of up to 25 μm and fumed silica. These are two-component systems which must be mixed with a curing agent before processing. The third adhesive is the film adhesive LOCTITE EA 9695 050NW Aero (Henkel AG & Co. KGaA, Düsseldorf, Germany) [17], which incorporates a polyethylene terephthalate (PET) carrier fabric that improves its manageability.

An investigation was carried out to characterize the individual components of the bond. For this purpose, tensile specimens were fabricated from the adhesive LOCTITE EA 9396 and the toughened epoxy resin 8552 (Hexcel Corporation, Stamford/CT, USA) [8], following the guidelines of DIN EN ISO 527-2 [18]. Initially, the adhesive respectively the resin was cross-linked in a casting mold in plate form in an oven. Subsequently, test specimens based on type 1B were milled from these plates. These have a length of 120 mm, a width at the narrowest cross-section of 10 mm, and a thickness of 2 mm. Six test specimens of each material were examined. The representative stress-strain curves are plotted in Fig. 3 (a). The position of the examined materials within the adhesive bond is visualized in Fig. 3 (b) which shows a cross-section through a bonded specimen. The depicted CFRP substrate was manufactured using a peel ply and therefore exhibits a distinct surface topography that determines the shape of the adhesive layer.

From the stress-strain curves, an elastic modulus can be determined for the resin 8552 of 4000 MPa and for the adhesive LOCTITE EA 9396 of 2735 MPa. This means that the stiffness of the resin is 1.46 times higher than that of the adhesive. For the adhesive LOCTITE EA 9396, a fracture strain of 8.2 % was determined, whereas for the resin 8552, it was found
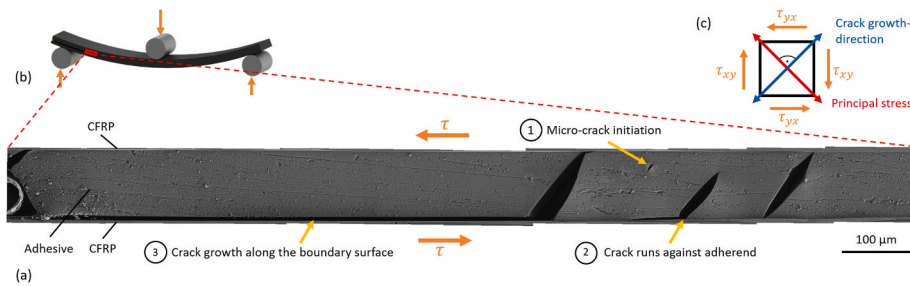
Fig. 4. (a) SEM cross-section image of a detail of the adhesive layer displaying crack formation at a load of −570 N. (b) Schematic representation of the ENF specimen. (c) Simplified depiction of the prevailing stress condition in the bondline.

to have a maximum at 4.9 %. While the resin exhibits a tensile strength of up to 101 MPa, the adhesive fails at 62 MPa.

2.3. Miniaturized in situ testing inside an SEM

For certifying CFRP components for aviation, the design of the mechanical tests is specified by the test pyramid, also known as the building block approach, in accordance with AMC 20–29 [19]. As the qualification level progresses, the complexity of the test specimens increases, while the number of specimens typically decreases. However, even at the lowest level the size of the test specimens is typically within a few centimeters, which means that effects at the micrometer scale can only be captured in a homogenized manner. As a result, the depth of insight provided by these types of specimens is limited.

An approach to address the heterogeneous microstructure of composite bonds and gain more detailed insights into processes at the micrometer scale is the *in situ* testing of miniaturized specimens in a SEM. A methodology for testing ENF specimens inside a SEM and analyzing them using digital image correlation was introduced by Diez et al. [14]. In this process, test specimens are subjected to load in the SEM while high-resolution images are captured. To enable digital image correlation, a stochastic pattern is generated on the specimen's surface through plasma etching. The plasma treatment creates fine structures on the specimen's surface, which generate contrast in the SEM image due to the edge effect. This can be utilized for pattern recognition to quantitatively capture deformations on the specimen.

Using this methodology, the influence of fillers and the morphology of CFRP adherends on the strain distribution in the adhesive layer was investigated. It should be noted that the presented results refer to individual test specimens. Therefore, it is not possible to provide a standard deviation for the absolute values of the individual strain distributions.

3. Results and discussion

3.1. Influence of surface morphology

In the following section, the influence of three distinct surface morphologies on the strain distribution and damage behavior within the adhesive layer is investigated: initially for flat adherends, followed by two differently structured adherends created using different top-layer peel ply fabrics.

Initially, the damage behavior of an unfilled adhesive layer in conjunction with a flat CFRP adherend was examined. The surface morphology was generated using the A5000 release film. In this test specimen, a metal insert with a thickness of 80 μm was employed both to control the adhesive layer thickness and to serve as an artificial crack. Consequently, due to the smooth adherend surface, the adhesive layer also measures precisely 80 μm in thickness.

Fig. 4 (a) illustrates the observed region of the adhesive layer adjacent to the artificial crack. The image depicts the state after damage initiation at a load of −570 N, simultaneously showing different co-occurring stages of crack evolution. The schematic representation of the ENF specimen is displayed in Fig. 4 (b), with a red marking indicating the area examined by microscope. Additionally, a simplified depiction of the prevailing stress condition in the bondline is provided in Fig. 4 (c), illustrating the direction of shear stresses, the principal stress, and the crack opening direction, which runs orthogonally to the principal stress [20]. When the specimen is subjected to loading, crack initiation occurs in the center of the adhesive layer. Subsequently, the crack propagates orthogonally to the principal stress in the direction of the two adherends. Due to the predominant shear stress, this corresponds to an angle of approximately 45° with respect to the adherends. Upon reaching the adhesive-resin interface, the crack continues to propagate along the surface of the adherends.

This configuration was analyzed using DIC, as described in chapter 2.3. The evaluation is depicted in Fig. 5, showing the SEM image overlaid with the calculated shear strains. Visualizations with two different color scaling parameters are presented to illustrate both the primary
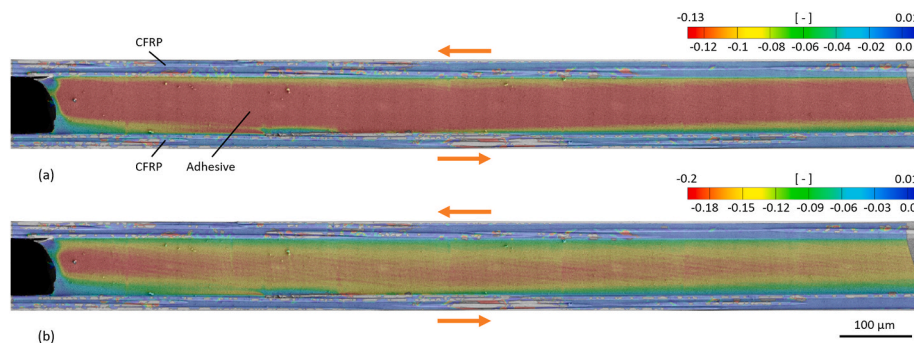

Fig. 5. SEM cross-section image overlaid with DIC calculation of shear strains at −400 N (A5000 morphology). (a) Scaling to visualize the areas of load transfer. (b) Scaling to visualize the load maxima.
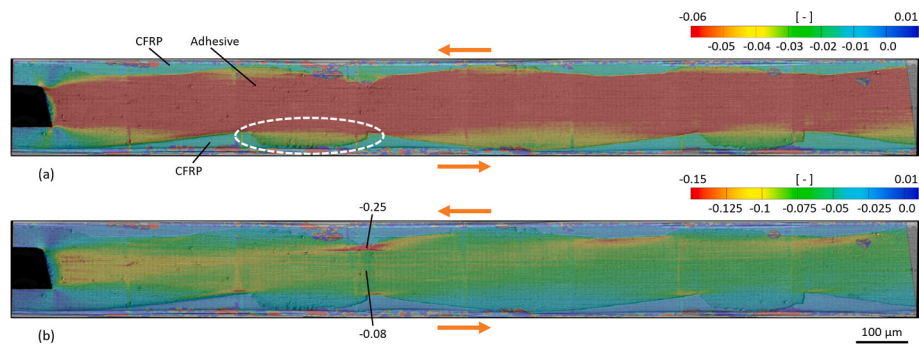
Fig. 6. SEM cross-section image overlaid with DIC calculation of shear strains at −400 N (ReleaseEase morphology). (a) Scaling to visualize the areas of load transfer. (b) Scaling to visualize the load maxima.
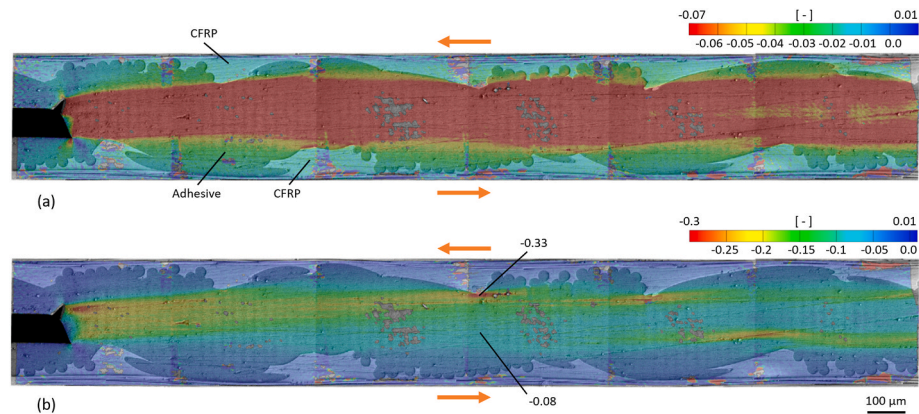

Fig. 7. SEM cross-section image overlaid with DIC calculation of shear strains at −400 N (08940 UTT morphology). (a) Scaling to visualize the areas of load transfer. (b) Scaling to visualize the load maxima.

load transfer path and the areas of maximum strain values. To highlight the primary load transfer area and visualize shear bands, the color scale's limit values were adjusted to clearly distinguish between regions of high and low load. Fig. 5 (a) shows that the load transfer and the associated strain occur uniformly along the adhesive layer, as indicated by a continuous shear band. A local delamination becomes visible on the lower adherend, affecting the strain distribution. In Fig. 5 (b), the DIC analysis reveals that the highest strain values occur in the center of the adhesive layer. This explains why crack initiation is found in the middle of the bondline. Their value decreases towards the adherends, with significantly lower strains found in the vicinity of the carbon fibers.

Now, a test specimen is examined whose CFRP adherends were produced using the peel ply ReleaseEase. The load corresponding to the illustrated strain distribution is again set at −400 N. The use of an 80 μm insert to adjust the adhesive layer thickness results in a bondline of 80 μm, measured from the highest elevations of the adherends. This indicates that the average adhesive layer thickness is higher than that of the previous test specimen. However, the DIC evaluation of the strains in Fig. 6 (a) reveals that the load transfer in the adhesive occurs between the maximum protrusions of the adherends. This implies that the area of load transfer, which can be described as the effective adhesive layer thickness, is comparatively large compared to the previous specimen.

Between the resin protrusions on the substrate surface, there are regions within the adhesive exhibiting significantly lower strain (as indicated by the ellipse in Fig. 6 (a)). This suggests that the structuring of the CFRP surface effectively redirects shear strain in the adhesive away from the adherends in certain areas. A possible explanation for this phenomenon is the variance in stiffness between the resin and the adhesive. As the tensile tests on the polymers have shown, the composite resin is significantly stiffer than the adhesive (see Fig. 3).

Another effect induced by the surface topography is depicted in Fig. 6 (b). Local shear strain maxima emerge within the adhesive at the tips of the adherends. At the localized load peak with the most pronounced manifestation, the shear strain value in the adhesive in the immediate vicinity of the peak of the adherend is −0.25, whereas the value at the center of the adhesive layer is −0.08. This corresponds to a shear exaggeration by a factor of 3.1.

The strain distribution at −400 N for a test specimen with a CFRP substrate produced using the 08940 UTT peel ply is illustrated in Fig. 7. The thickness of the artificial crack is 80 μm. Similar to the previously examined test specimen with the ReleaseEase topography, the strains primarily localize between the highest protrusions of the adherends within the adhesive. Likewise, there is excessive strain observed in the adhesive at the tips of the adherends, as depicted in Fig. 7 (b). Here, the shear strain value is −0.33, while the value at the center of the adhesive layer is −0.08. This corresponds to a shear exaggeration by a factor of 4.1.

It is noteworthy that the sharp-edged impressions of the peel ply in the recesses of the surface topography are not situated within the load-transferring area and consequently experience minimal strain. Therefore, there is no increased notch sensitivity associated with this geometry concerning the bond.

In addition to the test specimens featuring an adhesive layer thickness of 80 μm, specimens with a reduced adhesive layer thickness of 20 μm were also investigated. Similar effects were observed for these specimens. However, the formation of load maxima at the tips of the adherends and the onset of damage occurred at lower loads in specimens with the thinner adhesive layer.

The shear stress concentration at the protrusions of the adherends leads to crack initiation in these areas rather than in the center of the
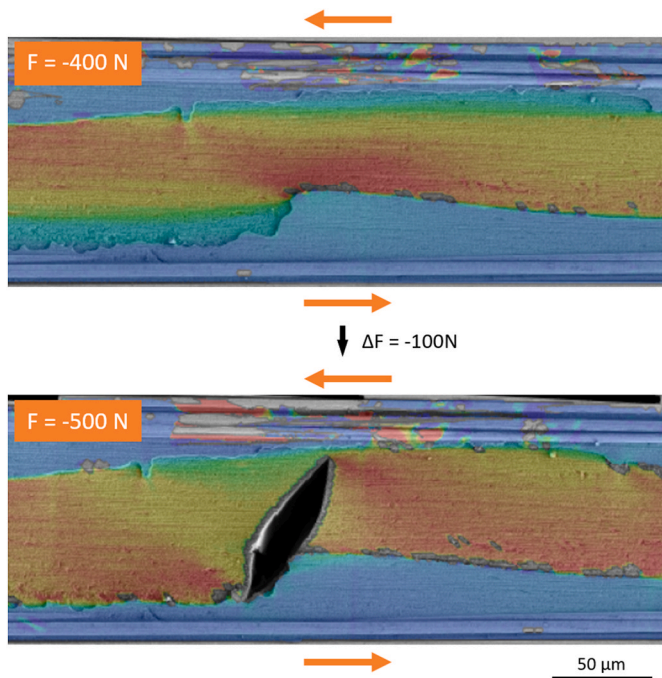
Fig. 8. Redistribution of strains during damage initiation (crack arrest effect).

adhesive layer, as observed in joints with smooth surface morphologies. In a test conducted using a test specimen featuring the ReleaseEase topography, a favorable redistribution of stresses at the onset of damage was observed. As depicted in Fig. 8, the adhesive exhibits low strain values in the area at the bottom left of the resin flank. Upon increasing the load from −400 N to −500 N, a microcrack initiates at the point of maximum shear strain, located at the protrusion of the adherend. Similar to the smooth adherend illustrated in Fig. 4, this microcrack propagates at a 45° angle relative to the surface of the adherend. However, at the lower adherend, the crack propagates into the region of low strain within the adhesive, prompting a redistribution of stresses and strains. This mechanism can be characterized as a crack arrest effect, as it results in the redistribution of stresses to areas previously unaffected by stress. In this way, the adhesive layer is capable of absorbing additional energy.

3.2. Mechanical effects of fillers on the microscale

Fillers are commonly employed in adhesives to facilitate their handling. Fillers can be utilized to achieve a desired adhesive layer thickness without the need for additional spacers. Glass beads, ceramic fillers, or fabrics are commonly used as spacers for this purpose. Fabrics, in particular, offer the advantage of not only controlling thickness but also lateral adhesive distribution. Adhesive films equipped with these spacers can be conveniently applied to the adherends, making them preferred for industrial applications. Another component of primarily paste-like adhesives is fumed silica. Fumed silica allows modification of the adhesive's flow properties. Its addition increases the viscosity of the adhesive and induces thixotropy, which is intended to prevent the adhesive from flowing out of the bondline [4].

For this study, ENF specimens were produced using a mixture of the adhesive LOCTITE EA 9395 and LOCTITE EA 9396. The adhesive LOCTITE EA 9395 contains both ceramic fillers made of silica and fumed silica. Fig. 9 shows detailed views of the adhesive layer at various shear load levels, captured using scanning electron microscopy. To enhance the visibility of the constituents of the bondline, the specimen was etched with low-pressure oxygen plasma beforehand. The sub-images display the adhesive layer and the adjacent surfaces of the adherends. Ceramic fillers are identifiable as bright areas within the adhesive, whereas the fumed silica appears slightly greyer and exhibits significantly smaller structures. Under load, even at a low level of −200 N, the cracking of larger fillers can be seen. The first resulting crack in the filler is indicated by a yellow arrow. Upon further increase in load, additional cracks and delamination of the fillers from the adhesive can be observed.

A larger area of the same specimen is depicted in Fig. 10. Here it can be seen that microcracking occurs uniformly throughout the adhesive layer, but only where large fillers are present. Additionally, an image of a further load level at −500 N is included, illustrating the progression from microcracks to the development of macroscopic cracks. The subsequent macroscopic failure of the specimen occurred at slightly more than −500 N.

To examine the micromechanical influence of the carrier fabric in the LOCTITE EA 9695 AERO film adhesive, ENF specimens were manufactured with this adhesive. CFRP laminates served as the adherends, which were prepared using the smooth release film A5000. Fig. 11 illustrates the adhesive layer in the region of the artificial crack and the adjacent adherends at various load levels. Delamination of the fabric fibers from the adhesive becomes noticeable at −300 N. By −400 N, these delaminations intensify, and additional delaminations become apparent. If the load is further increased, the microscopic delaminations merge to
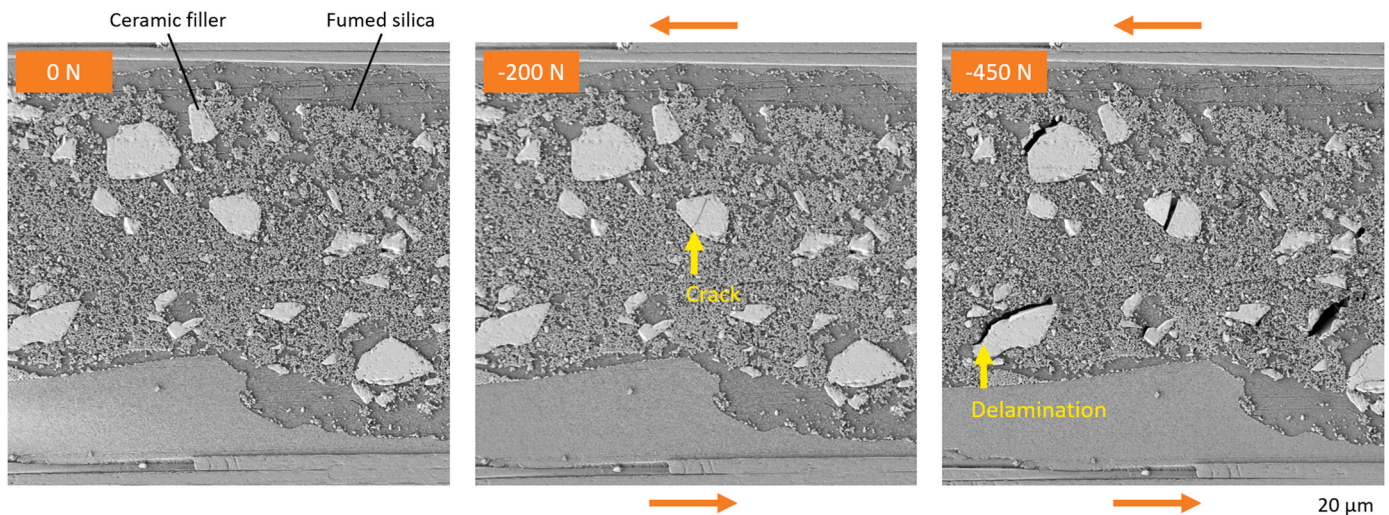

Fig. 9. Microcrack formation and delamination of fillers within a filled adhesive layer (SEM cross-section images captured at various load levels).
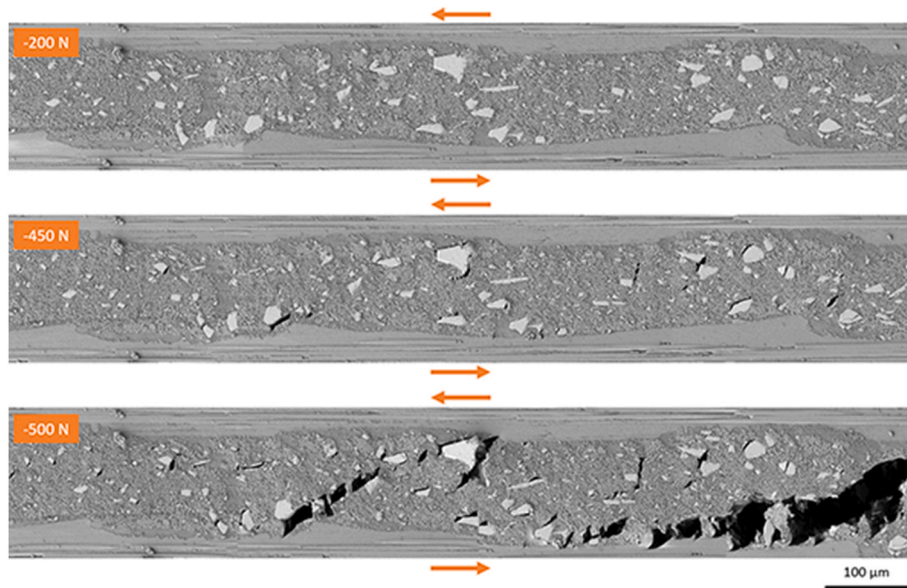
Fig. 10. Microcrack formation and subsequent merging to form macroscopic cracks within a filled adhesive layer (SEM cross-section images captured at various load levels).
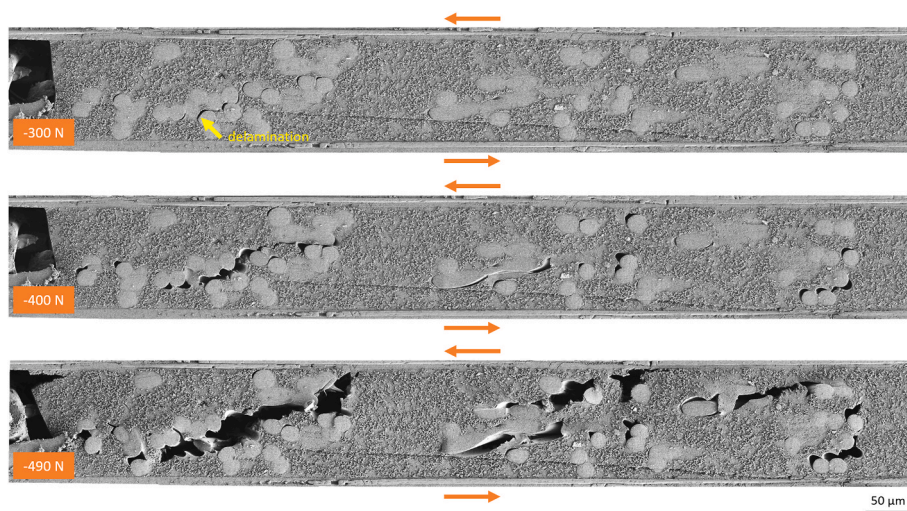

Fig. 11. Delamination of the PET carrier fabric within an adhesive layer (SEM cross-section images captured at various load levels).
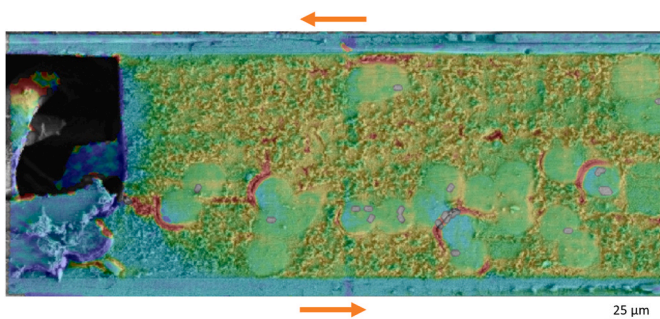

Fig. 12. Detailed view of the shear strain distribution within the adhesive layer at a load of −200 N.

form a macroscopic crack. Thus, it is evident that the fabric fibers can be regarded as predetermined weak points in the adhesive layer. In contrast to ceramic fillers, plastic fibers do not exhibit cohesive failure. This is due to their significantly higher ductility compared to ceramics. It is noteworthy that cracking tends to occur preferentially on clusters of carrier fabric fibers. From this observation, a direct correlation between the shear strength of this bondline and the uniformity of the distribution of the fabric fibers can be derived.

The region in the adhesive layer directly adjacent to the insert was also analyzed using digital image correlation. The shear strain distribution at a load of −200 N is depicted in Fig. 12. It can be seen that stress peaks form at the fiber-adhesive interfaces. With image correlation, these areas of high strain can already be identified, while the formation of microcracks is not yet or barely visible.

4. Conclusions

By examining adhesively bonded specimens under shear load in a SEM, it was possible to gain insights into micromechanical effects occurring within the adhesive layer and the regions adjacent to the surface of the adherends. The utilization of different semi-finished products in the production of CFRP results in distinct surface
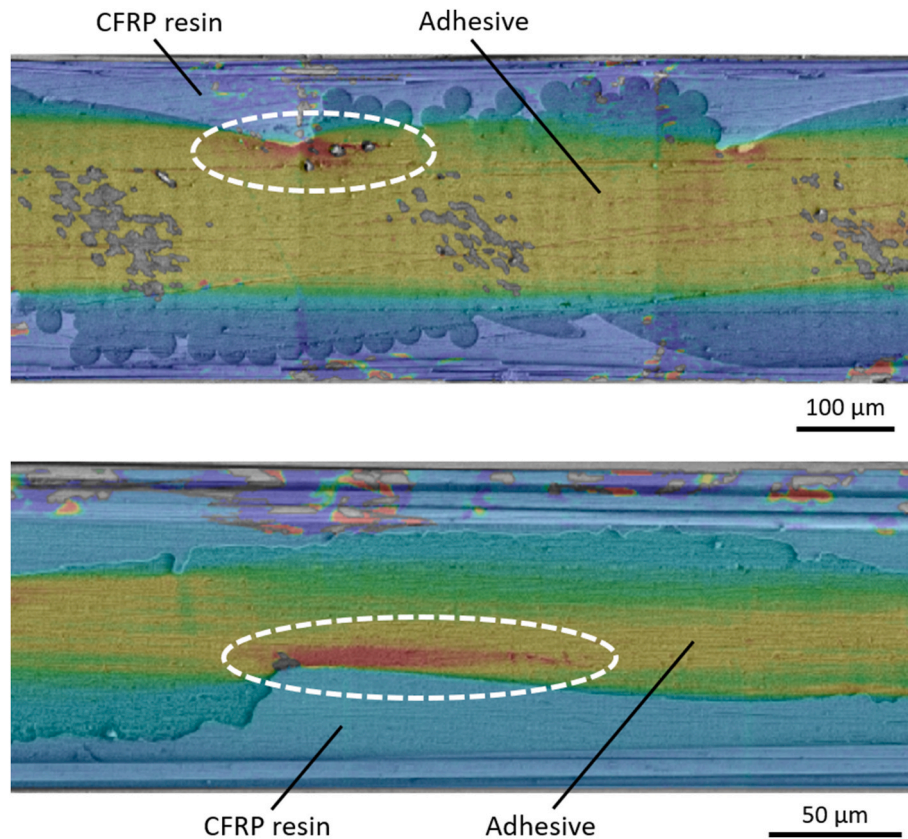
Fig. 13. Local load excesses within the adhesive at the protrusions of the adherend's topography.

morphologies of the adherends.

The examination of ENF test specimens has revealed that, in the case of structured adherend surfaces, the region of primary load transfer within the adhesive layer is largely isolated from the adherends. This region is bounded by the highest elevations of the adherend's topography, which consist of resin. Due to the higher stiffness of the CFRP resin compared to the tested adhesive, shear strain predominantly manifests within the adhesive. The largest occurring strains are only experienced near the highest points of the adherend's topography, leading to two distinct effects.

On the one hand, the adherend's morphology leads to the generation of local load peaks at the tips of the resin-rich surfaces (see Fig. 13). Different peel ply materials result in differently sharp protrusions on the CFRP, influencing the formation and height of these load peaks. The topography produced with the peel ply 08940 UTT causes more concentrated load peaks due to the sharper protrusions. This also creates a greater notch sensitivity compared to specimens with the topography produced using the ReleaseEase peel ply, which leaves very gently rising flanks on the CFRP.

Another effect of the adherend's morphology is the formation of areas filled with adhesive between the protrusions of the adherends, which, even under load, are subjected to low stresses and strains. If a crack occurs in the adhesive layer, it propagates at approximately a 45° angle counter to the surface of the adherend due to the prevailing stress state. However, if it encounters a region with low stress levels, a redistribution of load occurs, which is expected to slow down the propagation of the crack.

It is possible that the increased notch sensitivity associated with the 08940 UTT peel ply may diminish the advantage of load redistribution more significantly compared to the ReleaseEase peel ply. This could explain the higher durability of CFRP tensile single-lap shear specimens fabricated with a fine peel ply compared to those fabricated with the coarse peel ply 08940 UTT, as observed by Thäsler et al. [5].

Based on these findings, a finite element simulation can be employed to optimize the joint morphology. The goal is to preserve the crack arrest effect while minimizing stress peaks on the resin flanks.

The micromechanical behavior of the fillers in the adhesive layer under load was also investigated. It was observed that ceramic fillers can undergo both cohesive fracture and delamination from the adhesive. The resulting microcracks merge under increasing load to form a macroscopic crack. Also, delamination of the fibers from the adhesive was observed for the polymer carrier fabrics frequently used in film adhesives. This suggests that the fabric within the shear-loaded adhesive layer serves as a predetermined weak point. This effect is intensified when fibers are clustered within the adhesive layer. Here, it is worth investigating whether a surface pre-treatment of the PET fibers can improve bonding to the adhesive and how this affects the overall properties of the test specimen.

Publication funding acknowledgement

CRediT authorship contribution statement

Jörg Gregor Diez: Writing – original draft. **Jens Holtmannspötter:** Supervision. **Elisa Arikan:** Supervision. **Philipp Höfer:** Supervision.

Declaration of competing interest

The authors declare that they have no known competing financial interests or personal relationships that could have appeared to influence the work reported in this paper.

Data availability

Data will be made available on request.

References

[1] Pantelakis S, Tserpes K, editors. Revolutionizing aircraft materials and processes. Cham: Springer; 2020.

[2] Irving PE, editor. Polymer composites in the aerospace industry. Amsterdam, Heidelberg: Woodhead Publishing; 2015.

[3] Lengsfeld H, Mainka H, Altstädt V. Carbonfasern: herstellung, anwendung, verarbeitung. München: Hanser; 2019.

[4] Rasche M. Handbuch klebtechnik. München, Wien: Hanser; 2012.

[5] Thäsler T, Holtmannspötter J, Gudladt HJ. Surface topography influences on the fatigue behavior of composite joints. Key Eng Mater 2019;809:341–6. https://doi.org/10.4028/www.scientific.net/KEM.809.341.

[6] Chung DDL. Composite materials: science and applications. second ed. London, Heidelberg: Springer; 2010.

[7] Kar KK, editor. Composite materials: processing, applications, characterizations. Berlin, Heidelberg: Springer Berlin Heidelberg; 2017.

[8] Hexcel Corporation. HexPly 8552 product data sheet. 2023. Stamford/CT.

[9] Thull D, Zimmer F, Hofmann T, Holtmannspoetter J, Koerwien T, Hoffmann M. Investigation of fluorine-based release agents for structural adhesive bonding of carbon fibre reinforced plastics. Appl Adhes Sci 2019;7(1):2. https://doi.org/10.1186/s40563-019-0117-8.

[10] Da Silva LFM, Öchsner A, Adams RD, editors. Handbook of adhesion technology. Berlin, Heidelberg, Cham: Springer; 2011.

[11] Hart-Smith LJ, Redmond G, Davis MJ. The curse of the nylon peel ply. International SAMPE symposium and exhibition. 1996. p. 303–17.

[12] Holtmannspötter J, Czarnecki JV, Wetzel M, Dolderer D, Eisenschink C. The use of peel ply as a method to create reproduceable but contaminated surfaces for structural adhesive bonding of carbon fiber reinforced plastics. J Adhes 2013;89(2):96–110. https://doi.org/10.1080/00218464.2012.731828.

[13] Holtmannspötter J, Wetzel M, Czarnecki J von, Brucksch R. Ultra high-resolution imaging of interface layers. Adhesion Adhesives & Sealants 2013;10(4):22–7. https://doi.org/10.1365/s35784-013-0233-y.

[14] Diez JG, Holtmannspötter J, Arikan E, Höfer P. Combination of scanning electron microscopy and digital image correlation for micrometer-scale analysis of shear-loaded adhesive joints. J Adhes 2024:1–17. https://doi.org/10.1080/00218464.2024.2370788.

[15] Henkel Corporation Aerospace. Technical process bulletin LOCTITE EA 9395 AERO. seventh ed. 2013. Bay Point/CA.

[16] Henkel Corporation Aerospace. Technical process bulletin LOCTITE EA 9396 AERO. seventh ed. 2013. Bay Point/CA.

[17] Henkel Corporation Aerospace. Technical process bulletin LOCTITE EA 9695 AERO. ninth ed. 2013. Bay Point/CA.

[18] DIN EN ISO 527-2:2012-06. Kunststoffe - Bestimmung der Zugeigenschaften - Teil_2: Prüfbedingungen für Form- und Extrusionsmassen (ISO_527-2:2012); Deutsche Fassung EN_ISO_527-2. Beuth Verlag GmbH 2012. https://doi.org/10.31030/1860304. Berlin.

[19] EASA. Easy access rules for acceptable means of compliance for airworthiness of products, parts and appliances (AMC-20): AMC 20-29 composite aircraft structure. 2018.

[20] Erdogan F, Sih GC. On the crack extension in plates under plane loading and transverse shear. Journal of Basic Engineering 1963;85(4):519–25. https://doi.org/10.1115/1.3656897.